Digital Reconstruction of the Fish Inner Ear Reveals a Three-Dimensional Vector Landscape of Directional Sensitivity

Elijah K. Berger, Loranzie S. Rogers, Joseph A. Sisneros, and Julian L. Davis

Contents

OPEN ACCESS with major support from JASCO APPLIED SCIENCES

E. K. Berger (✉)
Department of Engineering, University of Southern Indiana, Evansville, IN, USA
e-mail: ekb4@illinois.edu

L. S. Rogers
Department of Molecular and Cellular Biology, Harvard University, Cambridge, MA, USA
e-mail: loranzierogers@fas.harvard.edu

J. A. Sisneros
Department of Psychology, Department of Biology, and the Virginia Merrill Bloedel Hearing Research Center, University of Washington, Seattle, WA, USA
e-mail: sisneros@uw.edu

J. L. Davis
Department of Engineering and Virginia Merrill Bloedel Hearing Traveling Scientist, University of Southern Indiana, Evansville, IN, USA
e-mail: julian.ly.davis@usi.edu

© The Author(s) 2026

A. N. Popper et al. (eds.), *The Effects of Noise on Aquatic Life IV*,
https://doi.org/10.1007/978-3-031-94229-7_167-1

Abstract

In aquatic environments, the spatial cues, such as interaural time and level differences that support sound localization in terrestrial vertebrates, are unavailable to fishes. Instead, fishes detect acoustic particle motion using three paired otolithic end organs of the inner ear (saccule, lagena, and utricle), each containing sensory hair cells with distinct directional orientations. While these organs are thought to play complementary roles in encoding sound direction, how their three-dimensional (3D) organization supports sound localization remains poorly understood. To address this gap, a 3D digital reconstruction of the inner ear in the plainfin midshipman (*Porichthys notatus*) was created by combining micro-CT digitizations of epithelial surfaces with high-resolution confocal maps of hair cell orientations. The reconstruction revealed that the saccule is dominated by rostral- and caudal-oriented hair cell bundles, whereas the lagena and utricle provide complementary coverage along the dorsal and ventral axes. Lateral directions were sparsely represented, suggesting reduced sensitivity to sound arriving from the sides. Notably, the rostral-caudal emphasis corresponds with behavioral observations that *P. notatus* preferentially orient toward frontal sound sources. This integrative modeling approach advances understanding of fish auditory function of the inner ear and offers a framework for testing how otolithic end organs collectively contribute to sound localization.

Keywords

Digital reconstruction · Hair cell · Plainfin midshipman · Sound localization

Introduction

Terrestrial vertebrates localize sound primarily through binaural comparisons of auditory cues, most notably interaural time differences (ITDs), which encode the relative arrival time of a sound at each ear, and interaural level differences (ILDs), which encode relative intensity (Kandel et al. 2021). These cues are highly effective in air but are markedly diminished in water, making them less informative for fishes and other fully aquatic vertebrates. The speed of sound underwater is approximately five times faster than in air, diminishing ITDs to near-negligible values for most fishes and aquatic invertebrates. Similarly, because the acoustic impedance of fish tissues is closely matched to that of water, ILDs are minimal for most fishes. Together, these physical constraints render the terrestrial binaural strategy poorly suited for fishes and necessitate alternative solutions for sound detection and localization (Van Bergeijk 1967).

In fishes, sound detection is mediated by three paired otolithic end organs, the saccule, lagena, and utricle, which provide an "inertial" mode of hearing (Popper and Edds-Walton 1995). Each end organ functions as a biological accelerometer, detecting particle motion associated with sound waves. Particle motion detection is achieved via a dense calcium carbonate otolith within the end organ that is

mechanically coupled to a sensory epithelium lined with directionally sensitive hair cells. When sound-induced particle motion causes differential movement between the otolith and the sensory epithelium, the directionally sensitive hair cells transduce this mechanical displacement into graded receptor potentials that encode both the direction and the magnitude of the stimulus. Distinct differences in orientation, morphology, and neural connectivity among the saccule, lagena, and utricle enable them to provide complementary directional sensitivities, forming the foundation for spatial hearing in fishes (Rogers et al. 1988; Schuijf and Buwalda 1975).

Previous anatomical and physiological work has demonstrated that the three otolithic organs of the fish inner ear are generally oriented along distinct spatial planes (Fay 1984; Popper and Lu 2000). This arrangement allows each end organ to sample different directional components of particle motion, together producing a more complete picture of the acoustic environment (reviewed in Hawkins and Popper 2018). Nevertheless, the strategies by which the brain integrates these multiple, directionally tuned inputs to estimate sound source location remain largely unresolved. According to proposed models (Popper et al. 1988; Rogers et al. 1988), sound localization may rely on vector weighting or the integration of directional signals from populations of hair cells across multiple sensory epithelia to derive a net particle motion vector. However, direct empirical evidence for such a mechanism remains limited. This challenge can be addressed by applying advanced 3D imaging techniques that capture the geometry of the sensory epithelia, enabling the precise mapping of thousands of hair cell bundle orientations across their complex, curved surfaces.

Traditional approaches have relied on two-dimensional directional sensitivity maps of hair cell orientation (Schulz-Mirbach et al. 2013). While informative, these planar representations oversimplify the spatial complexity of the sensory epithelia and obscure how directional vectors are arranged and integrated in three-dimensional space (Popper 1976). Such simplification limits our ability to understand how the auditory nervous system combines multiorgan inputs into coherent spatial estimates of sound.

To overcome these limitations, high-resolution digital reconstructions of otolithic end organs provide a transformative approach. These reconstructions preserve the curvature and full three-dimensional distribution of hair cell orientations, offering a more accurate representation of the "vectorial landscape" of directional sensitivity. Beyond descriptive anatomy, digital models also create opportunities for computational testing of sound localization strategies, including vector summation, vector weighting, or more complex population-coding schemes, under systematically manipulable conditions.

Here, the authors present methods for generating high-fidelity digital reconstructions of otolithic end organ hair cell orientations, using the plainfin midshipman (*Porichthys notatus*) as a model. These reconstructions allow visualization of the full three-dimensional organization of hair cell bundles across all three otolithic end organs. By capturing the complete geometry of these directional sensors, this work lays the groundwork for exploring how their collective orientations may support near-field sound source localization in the underwater environment.

Methods for Modeling

The reconstruction of the otolithic end organs in the present study integrated two primary anatomical datasets: (1) the three-dimensional (3D) geometry of otolithic end organ macular surfaces and (2) two-dimensional (2D) maps of hair cell bundle orientations patterns. This combined approach preserved the curvature of each sensory epithelium while also capturing the distinct groups of directional sensitivity represented within each macula. Together, these steps produced a digital framework suitable for computational modeling for directional hearing in the plainfin midshipman. The acquisition, processing, and integration of these anatomical datasets are described below.

Acquisition of 2D Hair Cell Orientation Patterns

Two-dimensional maps of hair cell bundle orientation were obtained from published sources. For the plainfin midshipman, utricular and lagenar hair cell orientation data were taken from Coffin et al. (2012), while saccular maps were derived from Lozier and Sisneros (2020). When such datasets were unavailable, maps were generated de novo using confocal microscopy imaging of fluorescently labeled hair cell bundles (Fig. 1a).

Digitization of the 2D maps was performed by overlaying a 100 μm x 100 μm grid onto each macula (Fig. 1b). Within each grid cell, a single vector was assigned to represent the dominant orientation of hair cell bundle polarity. Although this gridding procedure does not resolve local variability in hair cell density or micro-heterogeneity in polarity, it preserves the overall vectorial organization of the epithelium and enables downstream integration with 3D macular geometry.

Three-Dimensional Macular Geometry

To determine the curved geometry of each end organ macula, a midshipman specimen was stained with 5% phosphotungstic acid (PTA) following Schulz-Mirbach et al. (2013) and scanned at 7.24 μm resolution using a Skyscan1172 micro-CT scanner. The epithelial surfaces of the saccule, lagena, and utricle were then manually segmented using 3D Slicer (https://www.slicer.org/). Surface meshes of the segmented maculae were exported as stereolithography (STL) files, which contained 3D coordinate information. For each STL mesh, a curved planar surface was estimated using a least-squares fitting algorithm. This method generated smooth mathematical representations of the epithelial surfaces (Fig. 1c), which were necessary for projecting hair cell orientation data into 3D space.

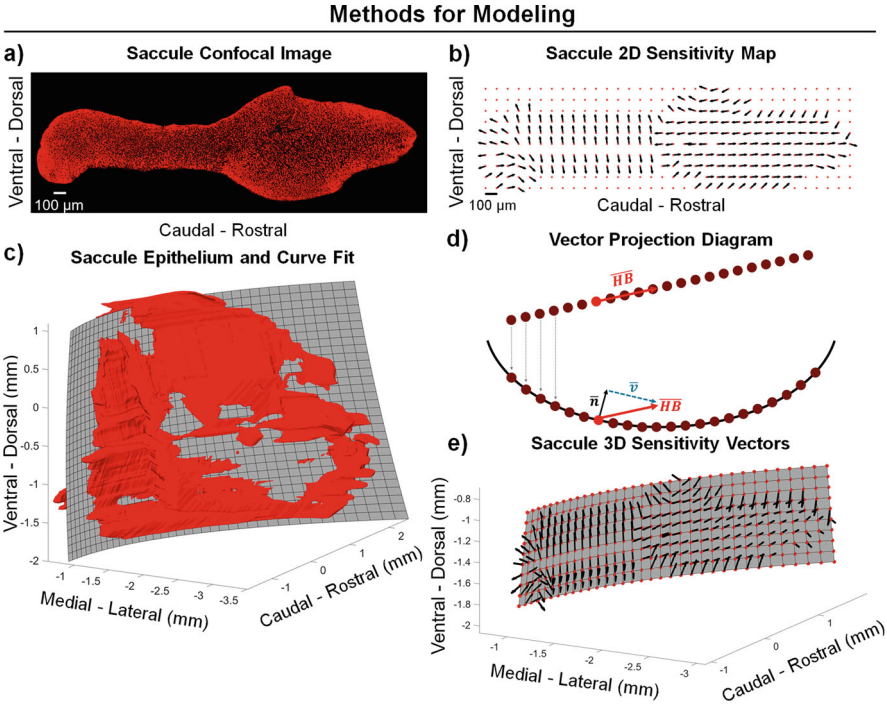

Fig. 1 Workflow for modeling the otolithic organs in plainfin midshipman. (**a**) Confocal image of the saccule macula showing hair cell bundles. (**b**) Digitized sensitivity map of the saccule derived from confocal images. Red dots represent points on a 100 µm × 100 µm grid. Black vectors indicate representative orientation vectors for each grid area with hair cell present. (**c**) Three-dimensional reconstruction of the saccular epithelium. The red body shows the saccular epithelium obtained via micro-CT scanning. The gray surface represents the least-squares curved plane fit to the epithelium, providing a mathematical approximation of epithelial geometry for subsequent projection of sensitivity vectors. (**d**) Schematic of the vector projection procedure. Red dots represent grid points from panel b, and the black curve denotes the fitted epithelial surface. At each grid point, the surface normal vector ($\overline{n}$) is calculated. The red vector $\overline{HB}$ represents the original 2D sensitivity orientation translated onto the 3D surface. Removal of the surface-normal component and normalization yields the corrected tangent vector (blue), which aligns with the local curvature of the macula. Gray arrows indicate the process of projecting 2D sensitivity vectors into 3D space. (**e**) Final 3D reconstruction of saccular sensitivity vectors. Red dots correspond to projected grid points, the gray surface shows the least-squares plane of the epithelium, and the black arrows represent the unit vectors tangent to the curved epithelial surface. Together, these steps generate a 3D sensitivity map suitable for bilateral reconstruction and computational modeling of directional hearing

Integration of 2D Orientation Maps with 3D Macular Geometry

The digitized 2D orientation maps were manually aligned with their corresponding macular STL surfaces. Using the equations for the best-fit curved planes, each 2D sensitivity vector was projected onto the 3D macular surface. This step correctly translated vector positions but initially retained their planar orientations.

Because hair cell bundle sensitivity is tangent to the macular surface (perpendicular to the stereocilia of each hair cell), vector orientation was corrected by removing the surface normal component of each vector and normalizing the result. This adjustment ensured that all sensitivity vectors lay tangent to the local curvature of the macula (Fig. 1d). The resulting set of unit vectors represented the properly oriented local directional sensitivity of each macula in 3D.

Bilateral 3D Digital Reconstruction of Hair Cell Sensitivity

The vector projection procedure yielded complete 3D directional sensitivity maps for the saccule (Fig. 1e) and, subsequently, for the lagena and utricle (data not shown in Fig. 1). After generating a full reconstruction for one ear, the model was mirrored across the midline to produce the contralateral ear. This resulted in a bilateral digital reconstruction of hair cell directional sensitivity across all three otolithic organs. The reconstructed dataset provides a structural basis for computational modeling of vectorial integration, enabling analyses of how populations of hair cells across the inner ear contribute to directional hearing in fishes.

Created Model and Results in Plainfin Midshipman

Once the complete set of 3D sensitivity vectors was calculated for each otolithic end organ, the vectors were translated to a common origin to facilitate direct comparison across structures. This transformation enabled the entire vector field to be visualized together in 3D space, revealing both regions of dense directional coverage and areas where sensitivity was sparse or absent. The model can be rotated and examined from multiple perspectives, dorsal, lateral, and frontal (Fig. 2), to evaluate spatial coverage patterns. These perspectives provide complementary insights into how the three end organs interact to represent sound direction. By plotting the saccule, lagena, and utricle simultaneously, the reconstruction highlights how each end organ contributes to distinct regions of the vector field, thereby supporting hypotheses of complementary functional specialization across the inner ear.

To quantify directional coverage, the 3D sensitivity vectors were binned into azimuth-elevation histograms (Fig. 3). Azimuth angles were grouped into 45° sectors around the fish's body axis, and each azimuth group was subdivided into 15° elevation bins. This binning allowed for systematic assessment of the relative contributions of the saccule, lagena, and utricle across the full spatial sphere.

Regional Patterns of Contribution

Rostral end **(azimuth: +45° to −45°)**—The saccule was the dominant contributor, with strong coverage at both vertical extremes(−90° to −75°) as well as the middle elevations (0° to +30°). Although less numerous, lagena and utricle vectors collectively spanned nearly the same vertical range: the lagena contributed to the extremes (low and high elevations: −90° to −45° and +60° to +75°), while the utricle filled the middle band(−60° to +60°).

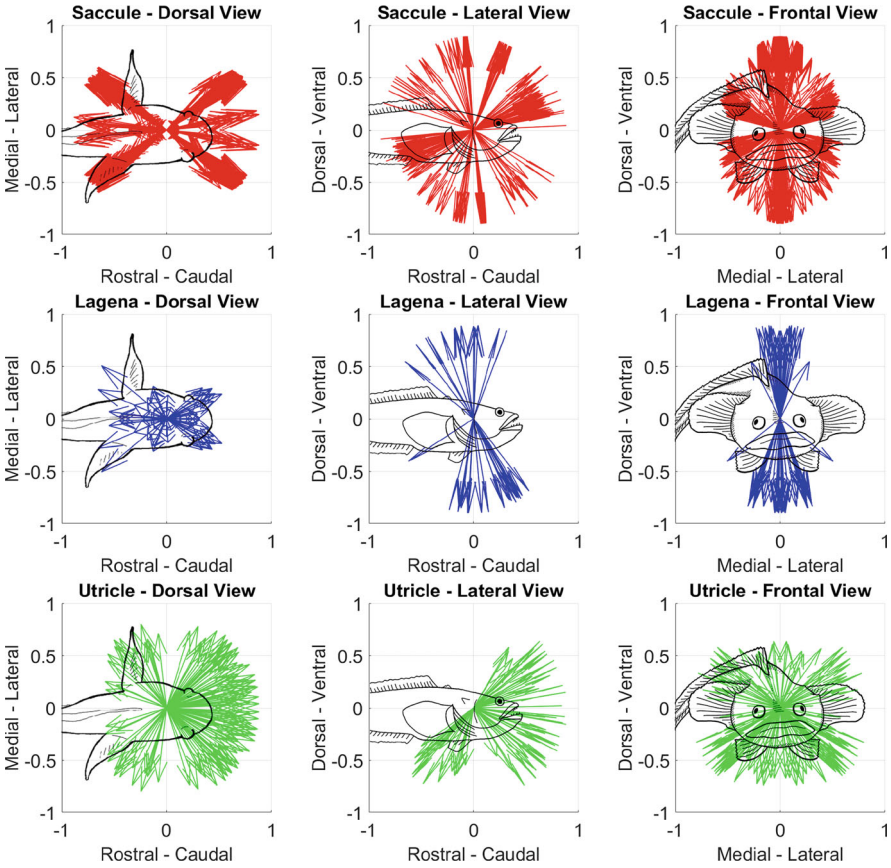

Fig. 2 Three-dimensional sensitivity vectors reveal complementary contributions of otolith end organs in the plainfin midshipman. Three-dimensional sensitivity vectors from the saccule (red), lagena (blue), and utricle (green), shown in dorsal (left column), lateral (middle column), and frontal (right column) views. All vectors are unit vectors (magnitude of 1) translated to a common origin, enabling direction comparison of spatial coverage. The visualization demonstrates organ-specific contributions to rostral, caudal, and lateral directions, with the saccule dominating along the rostrocaudal axis, the lagena occupying vertical extremes, and the utricle filling middle elevation ranges. Together, the three otolithic end organs provide partially overlapping but distinct directional sensitivity fields, while leaving spatial gaps that highlight potential blind spots in acoustic encoding

Rostral-lateral regions **(azimuth: +45° to +90° and −45° to −90°)**—Saccular input declined sharply, restricted to only the lower elevations(−60° to −30°). In contrast, the utricle dominated the middle elevations(−45° to +60°), while the lagena appeared mainly at the upper elevation extreme (+75° to +90°) but lacked coverage at lower levels. Notably, some bins in these sectors were empty, marking potential spatial "blind spots" in sensitivity.

Caudal-lateral regions **(azimuth: +90° to +135° and −90° to −135°)**—The saccule contributed no vectors in these quadrants. Coverage was overall sparse:

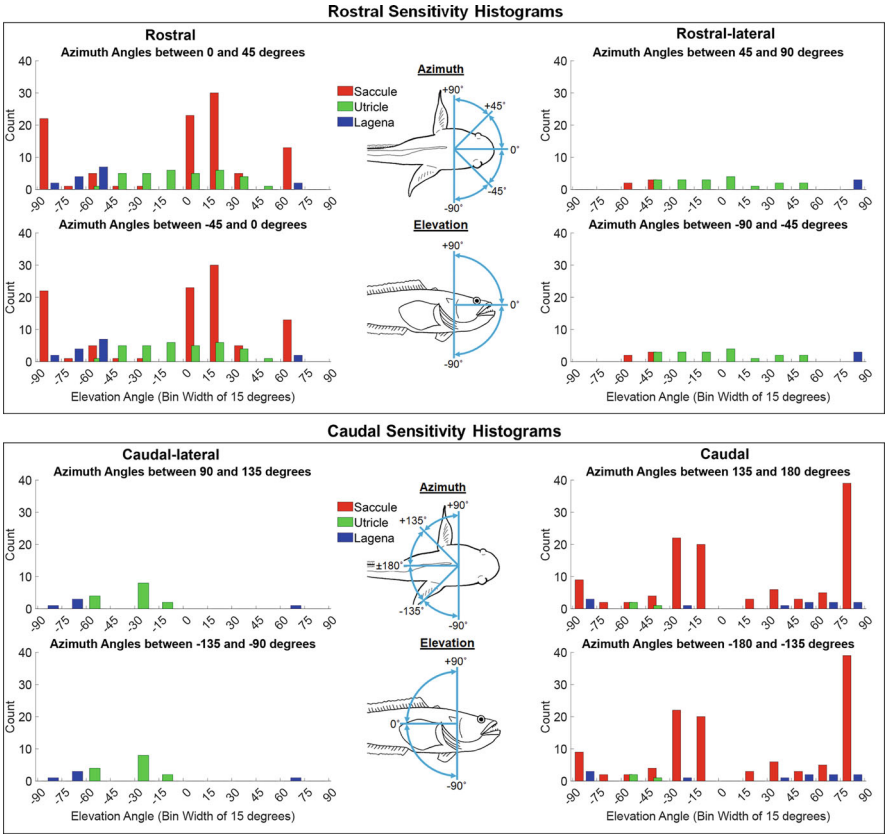

Fig. 3 Histogram analysis of directional sensitivity reveals complementary contributions of the saccule, lagena, and utricle. Top panels: Histograms are grouped by azimuth into rostral (azimuth: +45° to −45°) and rostral-lateral (azimuth: +45° to +90° and −45° to −90°) sectors. Rostral histograms are shown on the left, and the rostral-lateral histograms are shown on the right. Within each azimuth sector, elevation angles are subdivided into 15° bins, and the height of each bar represents the number of sensitivity vectors detected for that azimuth-elevation combination. Empty bins indicate spatial regions with no vector representation, i.e., directional "blind spots." Color coding denotes contributions from the three end organs: saccule (red), lagena (blue), and utricle (green). Bottom panels: Histograms for caudal-lateral (azimuth: +90° to +135° and −90° to −135°) and caudal (azimuth: ±135° to 180°) groups. Caudal-lateral histograms are shown on the left and caudal histograms on the right. This quantification highlights the complementary nature of otolithic end organ contributions: the saccule dominates the rostral and caudal sectors, particularly at vertical extremes; the utricle contributes most strongly to mid-elevation ranges, especially in lateral sectors; and the lagena preferentially represents vertical extremes across multiple azimuths. The presence of unfilled bins further underscores spatial discontinuities in directional encoding, suggesting that complete coverage of the acoustic field requires integration across all three end organs

the utricle was limited to portions of the middle elevations(−60° to −45° and −30° to −15°), while the lagena appeared at the lower(−90° to −60°) and upper (+60° to +75°) elevation extremes. However, large, uncovered gaps existed

across wide elevations bands, reinforcing lateral deficits in vector representation with limited or no coverage at −45° to −30°, 0° to +60°, and +75° to +90° elevations.

Caudal end **(azimuth: ±135° to 180°)**—Here, the saccule again dominated, contributing vectors across lower(−90° to −75°), middle(−30° to 0°), and upper elevations (+75° to +90°). As at the rostral end, the utricle and lagena combined to span much of the same vertical extent, pointing to a complementary distribution across end organs.

Summary of end organ contributions—Overall, the saccule was the primary end organ contributing to rostral and caudal sensitivity fields, consistent with its anatomical orientation. The utricle and lagena, by contrast, were more important for lateral coverage, with the lagena often occupying vertical extremes and the utricle dominating the middle elevations. The presence of empty azimuth, elevation bins, regions with no directional vectors from any organ, suggests the existence of spatial "blind spots" in end organ directional encoding.

Such blind spots in directional sensitivity may be potentially mitigated by natural behavioral sampling strategies employed during swimming. As fishes move forward, they often incorporate subtle oscillatory movements of the head and body, which effectively probe spatial variation in the surrounding acoustic field. These side-to-side head motions may help compensate for gaps in sensitivity by enabling the three otolithic end organs, each with hair cells tuned to distinct axes of particle motion, to dynamically sample across multiple dimensions. Through this process, the peripheral encoding of particle motion is integrated with active body movements, potentially reducing directional ambiguities. Although not yet directly tested, this dynamic interplay between sensory and behavioral mechanism could allow fishes to resolve sound direction with high fidelity, even in acoustically complex or noisy environments.

Conclusion

This study provides the first comprehensive three-dimensional digital reconstruction of otolithic end organ directional sensitivity in the plainfin midshipman, offering new insights on how the geometry of the saccule, lagena, and utricle support underwater sound source localization. By integrating high-resolution 3D macular surface geometry derived from micro-CT scans with 2D hair cell orientation maps obtained from confocal imaging, the complete spatial distribution of sensitivity vectors was visualized, and the contributions of each otolithic end organ were quantified across the range of azimuths and elevations.

The resulting reconstructions reveal that directional sensitivity is densest in the rostral and caudal directions, where all three otolithic end organs contribute and the saccule plays a particularly dominant role. This pattern aligns closely with the behavioral ecology of *P. notatus*, in which sound localization often requires orienting toward or away from conspecifics or other biologically relevant sources

located directly in front of or behind the animal (Zeddies et al. 2010). In contrast, lateral sectors exhibited sparser vector coverage and larger gaps, suggesting that reduced sensitivity in these regions may be of limited behavioral consequence. Notably, the oscillatory head and body movements characteristic of midshipman locomotion may help compensate for these gaps by allowing the fish to dynamically sample the acoustic field with its rostral end, where sensitivity is greatest.

Importantly, the empty bins in the azimuth-elevation histograms should not be interpreted as a complete absence of detection. Instead, these regions likely reflect reduced vector representation, which may still provide coarse directional cues or be supplemented by other sensory modalities (e.g., lateral line inputs or visual cues). Thus, while the otolithic end organ system exhibits a strong spatial bias toward forward-backward localization, it also maintains partial coverage of lateral fields, ensuring a robust representation of acoustic space in ecologically relevant contexts.

Overall, this digital reconstruction framework demonstrates how inner ear anatomy shapes directional hearing in fishes and establishes a methodological foundation for future comparative and functional studies. By applying this approach across taxa, researchers can begin to address broader questions about how otolithic end organ organization contributes to species-specific auditory capabilities, the evolution of vertebrate sound localization strategies, and the potential impacts of changing acoustic environments on aquatic life.

Acknowledgments The authors thank the organizers of the International Conference on the Effects of Noise on Aquatic Life, Prague 2025 for providing funding to Elijah Berger to present this paper at the conference. The authors also thank the editor Dr. Arthur Popper for his constructive feedback on the initial version and subsequent revisions of this review, which considerably improved the quality of the final version. This work was supported by the National Science Foundation (IOS 1933166 to JAS). LR was funded by the HHMUHanna Gray Fellowship and the Burroughs Wellcome Fund. JLD would like to thank the Virginia Merrill Bloedel Hearing Research Center and the University of Southern Indiana Provost Office for their support in this work. Open Access funding was provided by JASCO.

Competing Interest Declaration The author(s) has no competing interests to declare that are relevant to the content of this manuscript.

References

Coffin AB, Mohr RA, Sisneros JA (2012) Saccular-specific hair cell addition correlates with reproductive state-dependent changes in the auditory saccular sensitivity of a vocal fish. J Neurosci 32(4):1366–1376. https://doi.org/10.1523/JNEUROSCI.4928-11.2012

Fay RR (1984) The goldfish ear codes the Axis of acoustic particle motion in three dimensions. Science 225:951–954. https://doi.org/10.1126/science.6474161

Hawkins AD, Popper AN (2018) Directional hearing and sound source localization by fishes. J Acoust Soc Am 144(6):3329–3350. https://doi.org/10.1121/1.5082306

Kandel ER, Koester JD, Mack SH, Siegelbaum SA (2021) Auditory processing by the central nervous system. In: Kandel ER et al (eds) Principles of neural science, 6th edn. McGraw Hill

Lozier NR, Sisneros JA (2020) Ontogeny of inner ear saccular development in the plainfin midshipman (*Porichthys notatus*). Brain Behav Evol 95(6):330–340. https://doi.org/10.1159/000516477

Popper AN (1976) Ultrastructure of the auditory regions in the inner ear of the lake whitefish. Science 192(4243):1020–1023. https://doi.org/10.1126/science.1273585

Popper AN, Edds-Walton PL (1995) Structural diversity in the inner ear of teleost fishes: implications for connections to the Mauthner cell. Brain Behav Evol 46(3):131–140. https://doi.org/10.1159/000113266

Popper AN, Lu Z (2000) Structure–function relationships in fish otolith organs. Fish Res 46:15–25. https://doi.org/10.1016/S0165-7836(00)00129-6

Popper AN, Rogers PH, Saidel WM, Cox M (1988) Role of the fish ear in sound processing. In: Atema J, Fay RR, Popper AN, Tavolga WN (eds) Sensory biology of aquatic animals. Springer, New York, pp 687–710

Rogers PH, Popper AN, Hastings MC, Saidel WM (1988) Processing of acoustic signals in the auditory system of bony fish. J Acoust Soc Am 83(1):338–349. https://doi.org/10.1121/1.396444

Schuijf A, Buwalda RJA (1975) On the mechanism of directional hearing in cod (*Gadus morhua* L.). J Comp Physiol 98:333–343. https://doi.org/10.1007/BF00709804

Schulz-Mirbach T, Heß M, Metscher BD (2013) Sensory epithelia of the fish inner ear in 3D: studied with high-resolution contrast enhanced microCT. Front Zool 10(1):63. https://doi.org/10.1186/1742-9994-10-63

Van Bergeijk WA (1967) The evolution of vertebrate hearing. In: Neff WD (ed) Contributions to sensory physiology. Elsevier, pp 1–49

Zeddies DG, Fay RR, Alderks PW, Shaub KS, Sisneros JA (2010) Sound source localization by the plainfin midshipman fish, *Porichthys notatus*. J Acoust Soc Am 127(5):3104–3113. https://doi.org/10.1121/1.3365261

Open Access This chapter is licensed under the terms of the Creative Commons Attribution-NonCommercial-NoDerivatives 4.0 International License (http://creativecommons.org/licenses/by-nc-nd/4.0/), which permits any noncommercial use, sharing, distribution and reproduction in any medium or format, as long as you give appropriate credit to the original author(s) and the source, provide a link to the Creative Commons license and indicate if you modified the licensed material. You do not have permission under this license to share adapted material derived from this chapter or parts of it.

The images or other third party material in this chapter are included in the chapter's Creative Commons license, unless indicated otherwise in a credit line to the material. If material is not included in the chapter's Creative Commons license and your intended use is not permitted by statutory regulation or exceeds the permitted use, you will need to obtain permission directly from the copyright holder.